ADVANCED MATERIALS INTERFACES
www.advmatinterfaces.de

Funnel-Shaped Microstructures for Strong Reversible Adhesion

*Sarah C. L. Fischer, Katja Groß, Oscar Torrents Abad, Michael M. Becker, Euiyoung Park, René Hensel, and Eduard Arzt**

The potential of a new design of adhesive microstructures in the micrometer range for enhanced dry adhesion is investigated. Using a two-photon lithography system, complex 3D master structures of funnel-shaped microstructures are fabricated for replication into poly(ethylene glycol) dimethacrylate polymer. The diameter, the flap thickness, and the opening angle of the structures are varied systematically. The adhesion of single structures is characterized using a triboindenter system equipped with a flat diamond punch. The pull-off stresses obtained reaches values up to 5.6 MPa, which is higher than any values reported in literature for artificial dry adhesives. Experimental and numerical results suggest a characteristic attachment mechanism that leads to intimate contact formation from the edges toward the center of the structures. van der Waals interactions most likely dominate the adhesion, while contributions by suction or capillarity play only a minor role. Funnel-shaped microstructures are a promising concept for strong and reversible adhesives, applicable in novel pick and place handling systems or wall-walking robots.

1. Introduction

Fibrillar foot pad organs of many animals such as insects, spiders, and geckoes exhibit impressive adhesive performance to various substrates and have been studied by many research groups for almost two decades.[1–4] The improved understanding has triggered the desire to mimic the natural principles by creating synthetic, reusable polymer adhesives that show high potential for emerging applications.[5–12] The key is an optimized surface pattern tailored to the application that can be manufactured by techniques such as lithography, nanoimprint, or self-organization.[7,13–16] Patterned surfaces can exhibit better adhesion compared to nonpatterned counterparts, e.g., due to a higher compliance and, therefore, reduced elastic strain energy penalties and a higher conformability to various substrate topographies; these benefits have been termed the "contact splitting" effect.[2,17,18] The adhesion relies mainly on van der Waals interactions across the pattern–substrate interface. In addition, capillary forces may support the adhesive interaction.[19] van der Waals forces are significant only at short ranges, thus requiring intimate contact between the fibrils and the substrate. Based on the thermodynamic work of adhesion, theoretical pull-off stresses in the range of hundreds of megapascals have been estimated.[20,21] In practice, however, these stresses are typically in the range of several hundreds of kilopascals or below.[22–25] The discrepancy is most likely caused by nonideal contact and detachment conditions: possible causes are, besides surface roughness, unequal load sharing,[26] or flaws and local stress concentrations.[27–30] Therefore, tailoring the stress distribution along the fibril–substrate interface by reducing such stress concentrations is a major objective in fabricating synthetic fibrillar dry adhesives with high pull-off stresses.

Several experimental and numerical studies have already revealed that the tip shape of the fibrils strongly impacts the stress distribution. A conventional pillar structure with a constant axial cross-section exhibits a stress concentration at the edge of the contact area when the pillar is pulled normal to the surface, which always leads to detachment by edge cracks.[27,29,31,32] A prominent strategy to reduce the stresses at the edge is a gradual widening of the tip area, i.e., the formation of a so-called mushroom tip. Numerical studies have revealed that the magnitude of the stress singularity at the edge can be decreased by simultaneously increasing the stresses at the center of the contact.[29,31,33,34]

S. C. L. Fischer, K. Groß,[+] Dr. O. Torrents Abad, E. Park, Dr. R. Hensel, Prof. E. Arzt
INM – Leibniz Institute for New Materials
Campus D2 2, 66123 Saarbrücken, Germany
E-mail: eduard.arzt@leibniz-inm.de

S. C. L. Fischer, K. Groß,[+] Dr. O. Torrents Abad, Prof. E. Arzt
Department of Materials Science and Engineering
Saarland University
Campus D2 2, 66123 Saarbrücken, Germany

M. M. Becker
Fraunhofer Institute for Nondestructive Testing (IZFP)
Campus E3 1, 66123 Saarbrücken, Germany

E. Park
Department of Mechanical Engineering
University of California
Santa Barbara, CA 93106, USA

[+]Present address: University of Kaiserslautern, Department of Mechanical and Process Engineering, Erwin-Schrödinger-Strasse, Building 58, 67663 Kaiserslautern, Germany

The ORCID identification number(s) for the author(s) of this article can be found under https://doi.org/10.1002/admi.201700292.

DOI: 10.1002/admi.201700292

Practically, such a tip can be manufactured using anisotropic etching or by modifying tips of previously manufactured pillar structures, which results in significantly higher pull-off values compared to conventional pillars.[22,32,35,36] However, controlled generation of such tips remains difficult.

Another approach to modify the stress distribution is to vary the curvature of the pillar face coming into contact with the substrate. Convex (or conical) tips exhibit a parabolic stress distribution along the interface, but typically show low pull-off stresses due to the rather small contact area.[22,36,37] In contrast, concave or flat tips lead to higher contact areas in complete contact, thus these microstructures can exhibit larger pull-off stresses.[38,39] Gao and Yao theoretically demonstrated that such a concave tip geometry can lead to a homogeneous stress distribution.[30] Their calculations show that the edge stresses are reduced due to the fact that the edges are in compression while the inner contact area remains under tension. However, their approach requires very small curvatures, which are difficult to fabricate. In addition to the above mentioned concepts, triangular,[40] spatula-shaped,[41,42] and slanted tips[43,44] have been studied, introducing an asymmetry with potential improvements for directional or even switchable adhesion. Recently, we demonstrated that a combination of soft and stiff materials along the pillar axis improves the adhesion because the stress concentrations are reduced.[45] Furthermore, the soft component of the pillar, which is in contact with the substrate, may even increase adhesion to rough surfaces.[46]

In the present work, we introduce funnel-shaped microstructures that resemble a structural combination of mushroom- and concave-shaped tips. The microscale structures were fabricated using two-photon lithography and a subsequent replication technique to transfer the pattern into a soft methacrylate-based material. Adhesion of single structures was tested using a triboindentation system and was rationalized in terms of the geometric parameters of the funnel such as opening angle, flap thickness, and diameter of the structures. The attachment of the microstructures to the substrate was further observed in situ via scanning electron microscopy and theoretically elucidated by numerical simulations.

2. Results and Discussion

Funnel-shaped microstructures were successfully manufactured in a two-step process as shown in **Figure 1**c. A master template containing all 16 different microstructures was generated using two-photon lithography. By placing all structures on each sample, inhomogeneities and deviations induced by the manufacturing process and errors in the adhesion measurements induced by misalignment could be reduced. Cross-sections of all replicated microstructures were prepared to determine the real dimensions and the contact areas, which were further used to calculate pull-off stresses (Figure 1b,d).

A typical force–displacement curve obtained for a funnel-shaped microstructure is pictured in **Figure 2**a and can be divided into three characteristic regimes:

- Regime 1: During attachment, the compressive loading curve first exhibits a small slope that relates to elastic deformation and bending of the flaps. This slope (15.7 µN µm^{-1}) corresponds to an initially high compliance of the microstructures.
- Regime 2: With increasing load, the stiffness of the microstructures drastically increases, which is represented by a steeper slope (101.3 µN µm^{-1}). In addition to the deformation of the flaps, the stem of the microstructure was elastically deformed.
- Regime 3 corresponds to the unloading of the structures, which finally leads to detachment (156.8 µN µm^{-1}).

Adhesion measurements were repeated on each structure without significant damage or plastic deformation as shown in Video S1 (Supporting Information). In contrast to mushroom-shaped microstructures (Figure S1, Supporting Information), the pull-off stress of funnel-shaped microstructures depended on the indentation depth as exemplarily shown in Figure 2b. A similar behavior has already been reported for micropillars with concave faces by del Campo et al.[39] In fact, the initial contact of the flaps to the substrate led to an insignificant contact area with negligible adhesion. Only upon bending and stretching of the flaps did the whole structure form intimate contact with the substrate and were high pull-off forces obtained as reported in Figure 2b.

Figure 3a shows the force–displacement curves for structures with different opening angles but similar diameter (D = 15 µm) and flap thickness (d = 1 µm). Both the 120° and 90° structure exhibited the three characteristic regimes described above, while for the 180° structure, i.e., the mushroom structure, regime 1 could not be detected, as expected. For regime 3, a very similar behavior of all microstructures was obtained, characterized by an almost linear initial decrease in stress (2.39 MPa µm^{-1} for the structures with 15 µm diameter) and similar initial slopes of the unloading curves irrespective of their opening angles. This observation indicates that the contact stiffness of the attached microstructures was similar. For the structures with an opening angle of 120°, the unloading curve until detachment is almost linear; this indicates that the contact area remained constant because partial detachment or crack propagation would result in a decrease of stiffness. For the structures with 90° opening angle, we observed a gradual decrease of stiffness during unloading, which most likely reflects a continuous detachment.

The determined pull-off stresses are shown as a function of size and shape of the microstructures in Figure 3b. For example, microstructures with 15 µm diameter and 1 µm flap thickness and opening angles of 90° and 120° exhibited pull-off stress values of 1.7 ± 0.2 and 5.6 ± 0.2 MPa, respectively. That is, one order of magnitude larger compared to 112 ± 7 kPa for the mushroom-shaped structure with 180° opening angle as a control. To provide an overview of the geometric variations, cross-sections of all structures are shown in Figure 1d. Funnel-shaped structures with comparable compact tip shape, for example, diameter of 5 µm and flap thickness of 3 µm, resulted in low pull-off stresses most probably due to insufficient flexibility of the flaps. The flexibility of the flaps increased with higher flap length to thickness ratio, which, in turn, enabled intimate contact and, therefore, high pull-off stresses. Figure 3c illustrates the relationship between the pull-off stresses obtained and the aspect ratio, defined as the radius of contact divided by the flap

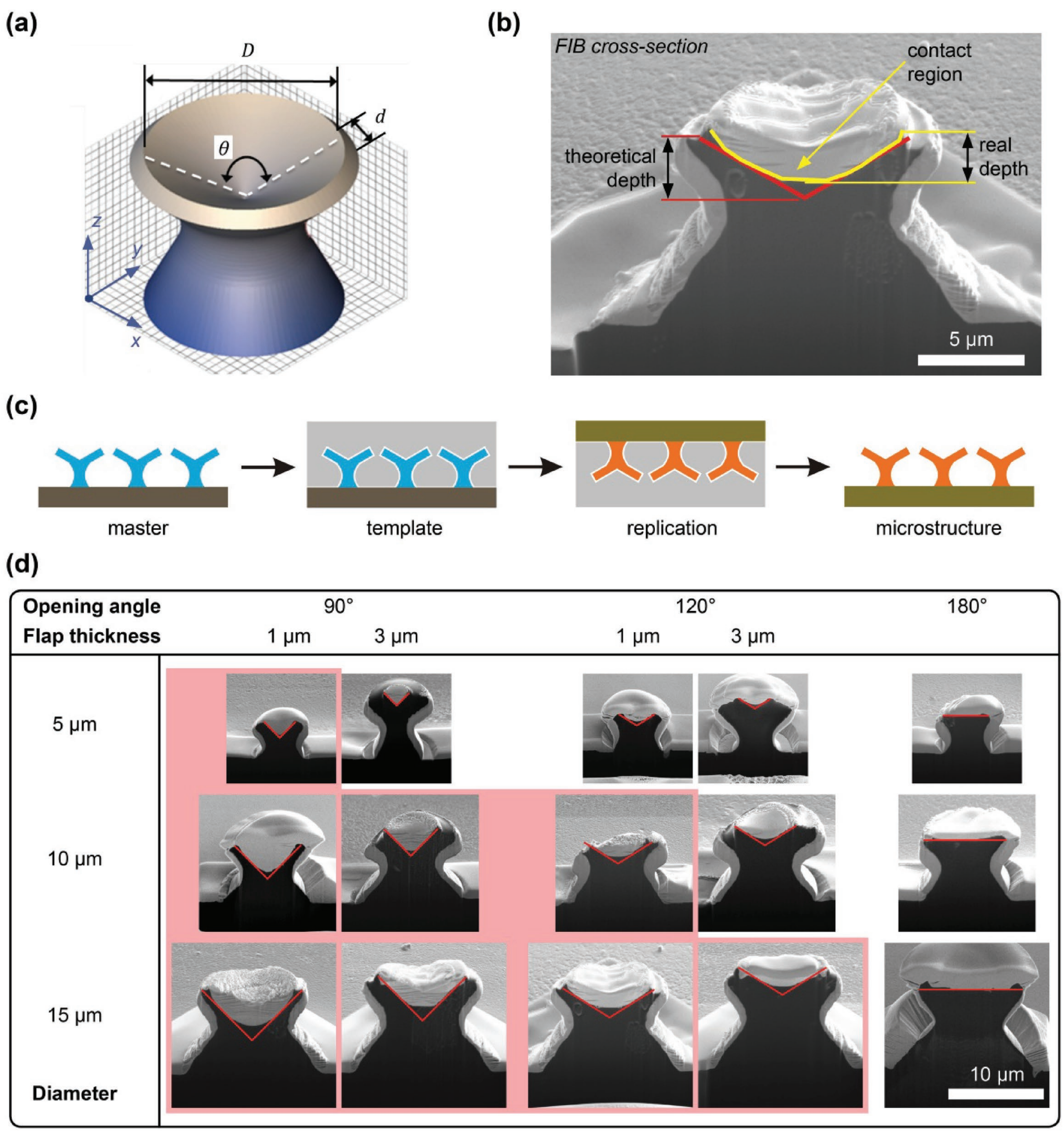

Figure 1. Funnel-shaped microstructures. a) 3D-CAD model for two-photon lithography. The diameter, D, the flap thickness, d, and the opening angle, θ, of the funnels were systematically varied. b) Scanning electron image of a FIB cross-section (D = 15 µm, d = 1 µm, θ = 120°). Bright: platinum deposit. The depicted real structures (yellow contour line) differed from the CAD model (red contour line) due to material shrinkage. c) Schematic of the double molding steps. Master structures (blue) were fabricated using two-photon lithography on a glass substrate and replicated into PDMS (grey). This template was in turn used to fabricate the funnel-shaped structures out of PEGdma (orange). d) Secondary electron images of FIB cross-sections. The structures exhibiting pull-off stresses higher than 1 MPa (see Figure 3b) are highlighted in light red. The red lines are intended to guide the eye and show the theoretical opening angle.

thickness, for all geometries. For aspect ratio of ⩾2, the structures exhibited pull-off stress values higher than 1 MPa as highlighted by the light red boxes in Figures 1d and 3b,c.

The shape of the microstructures might lead to the conclusion that the main contribution to adhesion is based on suction. However, the adhesive stress induced by suction, σ_{suc}, is limited by the atmospheric pressure of $p_{atm} \approx 100$ kPa. Hence, its maximal contribution to the pull-off stress is more than one order of magnitude smaller than the values obtained. In addition, experiments comparing adhesion under normal and reduced pressure of about 1.5×10^{-3} Pa were performed in situ with the nanoindenter. The pull-off stress obtained was only 30% lower than under ambient conditions as shown in Figure 3d, which demonstrates that suction plays a insignificant role.

Due to the hydrophilic nature of the polymer material, capillary forces might contribute to the adhesion.[47] The adhesive stress induced by capillarity, σ_{cap}, can be estimated as follows: $\sigma_{cap} \approx \frac{2L \cdot \gamma \cdot \cos\theta}{2A} + \frac{2\gamma}{R}$, where L is the length of the three-phase contact line, γ is the surface tension of water, θ is the contact angle, A is the contact area, and R is the radius of the fluid meniscus. We assume ideal wetting (θ = 0°), a thickness of

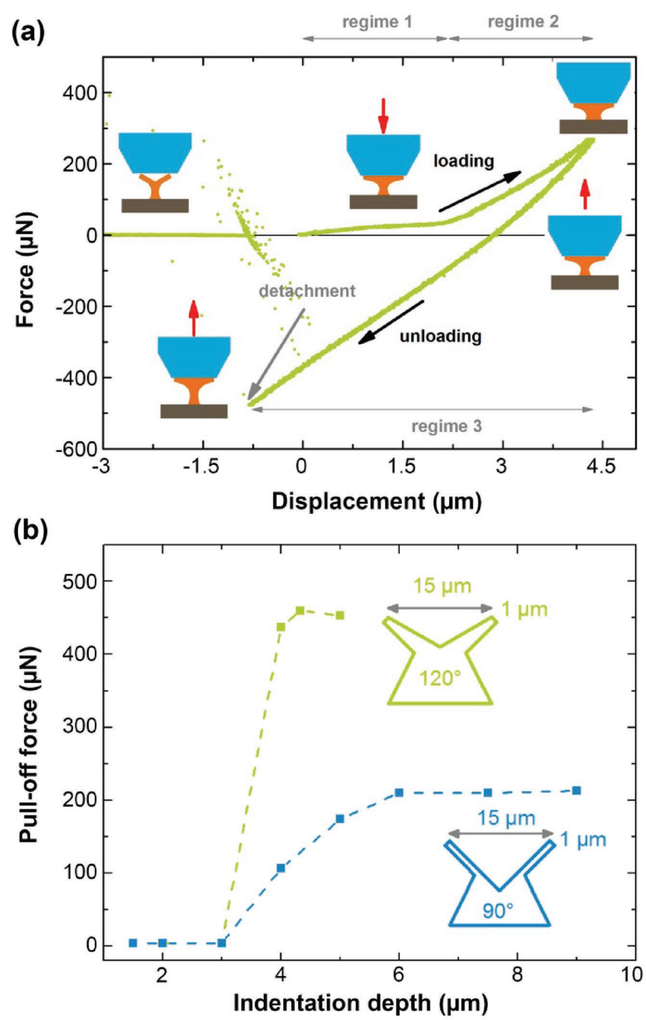

Figure 2. Typical force–displacement curve and pull-off force as function of indentation depth. a) The compressive loading curve (positive force) often comprises two parts with different slopes corresponding to bending of the flaps (regime 1) transitioning into compression of the whole structure (regime 2). The unloading curve (negative force values, regime 3) terminates in a maximal tensile force, indicating the pull-off force. The scattered data upon detachment are artifacts due to vibrations of the indenter. b) Pull-off force as a function of the indentation depth for two PEGdma600 microstructures with 15 µm diameter, 1 µm flap thickness, and opening angles of 120° (green) and 90° (blue).

the fluid film, h, that is much smaller than the radius of the meniscus ($h \approx R/100$) and use values from focused ion beam (FIB) cross-sections to determine the contact area. The resulting estimate of a capillary contribution is about 50 kPa, which is significantly smaller than the measured pull-off stresses.

Interestingly, the pull-off stresses obtained exceed by far the values of mushroom-shaped microstructures reported here and in the literature.[48,49] Such a result is unexpected because deformation of the flaps stores elastic energy, which could act against interfacial adhesion. The following possible explanations can be put forward:

1. Increase of real contact area: The highly compliant flaps may lead to better adaptation of the structures to slight irregularities on the substrate surface or to small misalignments. Particularly, the gradual contact formation from the edge of the flaps toward the center of the structure most likely ensures intimate contact over the whole contact area. This can possibly increase the real contact area over the case of mushroom structures with the same diameter in contact. In the unloading regime, the prior deformation of the flaps might induce frictional components that further increase adhesion as known from insects,[50] geckoes,[51] and artificial systems.[52]
2. Stress distribution: Funnel-shaped microstructures exhibit compressive stresses at the edge of the structure. As will be shown below, the magnitude of stress singularities at the edge is most probably reduced, which can have a beneficial impact on the pull-off stress.[33]

Figure 4a shows the normal stresses in vertical direction at selected deformation steps for different opening angles. For the mushroom structures (opening angle of 180°), normal stresses were the highest at the center and reduced at the corner of the structure immediately upon contact (indentation depth 1000 nm), in agreement with literature.[29,31,33] For the funnel-shaped microstructures, the results demonstrate the elastic flap deformation in accordance to the previously described regime 1 (Figure 2a). At the beginning of the compressive loading, the structure exhibited only a small contact area. With increasing indentation depth, the flaps deformed and induced two opposing stress regions, i.e., a tensile stress field on the substrate-facing side of the flaps (red region) and a compressive stress field on the opposite side (blue region). Between both regions, a stress-free zone formed. The compressive stresses in the stem were lower compared to the mushroom structure. In addition to the stresses inside the structures, the interfacial stresses varied characteristically between the funnel-shaped structures and the mushroom structures (Figure 4b). For the mushroom structure, the maximum interfacial stress was always located close to the center (I). In contrast, the flaps of the funnel-shaped structures induced an interfacial compressive stress concentration (II) that shifted radially from the edge (i.e., the location of initial contact) toward the center (III), while the contact area increased simultaneously. For similar indentation depths, the stress distributions of the 120° and 90° structures differ in magnitude and lateral position of the stress minima. For the 90° structures, small normal stresses reflect the high compliance of the structure during attachment in regime 1 in accordance to the experiments (Figure 3a). In addition, shear stresses resulting from the radial elongation of the flaps might also play an important role in adhesion, but could not be captured with our calculations.

Gao and Yao[30] reported on concave tip curvatures as a structural concept for uniform interfacial stress distribution by reducing corner singularities in particular. In their theoretical work, adhesion of pillars with concave faces and varying pillar size was calculated. For small pillar diameters (<100 nm), the pillars formed complete contact with the substrate immediately upon contact without preload. For larger pillar diameters (>100 nm), in contrast, complete contact could be only established upon exceeding a certain threshold of preload (or indentation depth), which is in accordance with our experimental findings and previous reports.[39,53] In addition to the

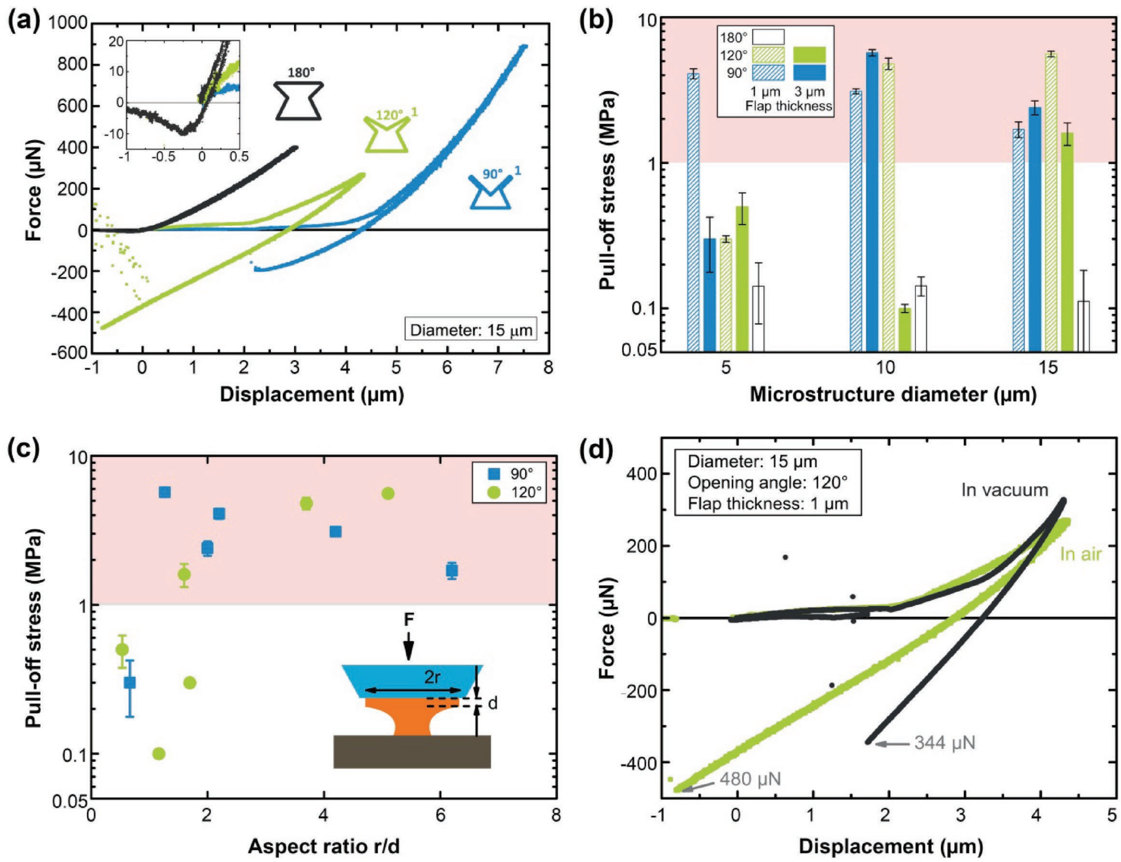

Figure 3. Detachment behavior measured for the different microstructures. a) Force–displacement curves for microstructures with diameter of 15 µm and flap thickness of 1 µm and different opening angles of 180° (black), 120° (green), and 90° (blue). The inset shows the force–displacement curve of the mushroom-shaped structure (opening angle 180°) in detail. b) Pull-off stresses as a function of diameter, flap thickness, and opening angle. Results for 1 and 3 µm flap thickness are shown in shaded and full color, respectively. c) Pull-off stresses as a function of aspect ratio, i.e., contact radius divided by flap thickness, for opening angles of 120° (green, circles) and 90° (blue, squares). The light red area highlights the pull-off stress ranging above 1 MPa in both (b) and (c). d) Force–displacement curve under ambient conditions (green) and under reduced pressure at about 1.5×10^{-3} Pa (dark green), both performed in situ with the picoindenter. Reported values represent the pull-off forces.

concave curvature, the funnel-shaped microstructures exhibit flaps similar to that known from mushroom-shaped structures. We believe that the funnel-shaped microstructures combine the structural concept of concave-shaped pillars with that of mushroom structures to result in high pull-off stresses. However, the attachment process to the substrates including the transition from a nonadhesive to a highly adhesive state is of fundamental importance in understanding these structures.

3. Conclusion

In the present work, we introduced funnel-shaped microstructures as a novel structural concept for strong and reversible patterned adhesives. We successfully demonstrated the generation of such structures using two-photon lithography and nanoimprint technique.

In summary, we can conclude:

– The pull-off stresses obtained reached values up to 5.6 MPa for single microstructures, which is, to the best of our knowledge, higher than any values reported in literature for artificial dry adhesives. It is expected that also arrays of funnel-shaped structures will surpass arrays with other geometries although arrays generally tend to show lower adhesion than single microstructures.[26]
– Tests under reduced pressure revealed that most probably van der Waals interactions contribute to the adhesion, while contribution of suction and capillarity plays only a minor role.
– The flexibility of the flaps provides high compliance during contact formation that helps to accommodate surface irregularities and even small misalignments between the structure and the substrate.
– The exceptionally high adhesion is very likely based on an enhanced real contact area due to gradual attachment from the edge toward the center of the structure. We also argue that the interfacial stress distribution is more conducive to adhesion in these structures.
– Our funnel-shaped microstructures resemble a synthesis of concave tip curvature as theoretically advanced by Gao and Yao[30] and mushroom-shaped structures including highly compliant flaps for intimate contact formation and strong adhesion.

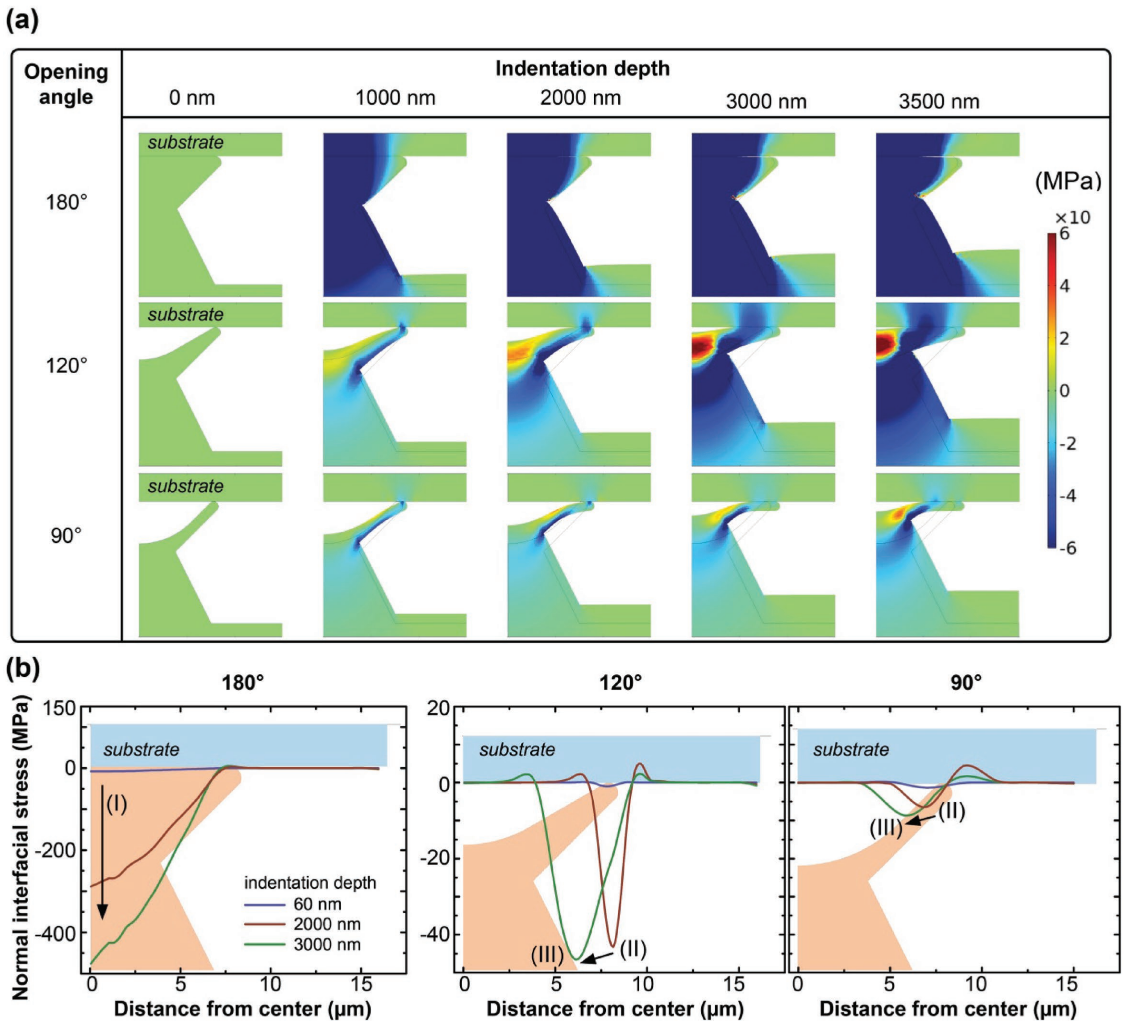

Figure 4. Results of finite element simulations. a) Normal stresses inside the microstructures, with different opening angles, and the substrates at different indentation depths. During attachment (compressive preloading), the images represent a half cross-section of the axisymmetric finite element (FE) model. Maximal compressive and tensile stresses are shown in blue (negative) and red (positive), respectively. Neutral stress regions are shown in green. b) Normal interfacial stress as function of indentation depth: 60 nm (blue), 2000 nm (red), and 3000 nm (green). The characteristic features and trends of the stress distributions are marked with arrows.

The paper shows that substantial improvement of dry micropatterned adhesive can still be expected from structure designs with optimized shapes.

4. Experimental Section

Microstructure Fabrication: CAD models (Figure 1a) of different funnel-shaped microstructures were designed and generated on a glass substrate using a two-photon lithography system (Photonic Professional GT, Nanoscribe, Eggenstein-Leopoldshafen, Germany) and the photoresist IP-L 780 (Nanoscribe, Eggenstein-Leopoldshafen, Germany). Three geometric parameters of the funnel-shaped tips were varied as follows (see Figure 1d): diameter (5, 10, and 15 µm), flap thickness (1 and 3 µm), and opening angle (90°, 120°, and 180° as a mushroom-shaped control structure).

Upon writing, the structures were developed in propylene glycol monomethyl ether acetate (STBD8433X, Sigma-Aldrich, St. Louis, Missouri, USA) for 20 min and subsequently rinsed in isopropanol for 2 min. The IP-L master structures were coated with (1H,1H,2H,2H-perfluorooctyl) trichlorosilane (AB111444, ABCR, Karlsruhe, Germany) in a vapor deposition process to ensure a low energy and nonreactive surface for replication into PDMS. IP-L master structures and 50 µL of the silane were placed in a vacuum chamber for about 60 min at reduced pressure and then used without any post treatment. PDMS (Sylgard 184, Dow Corning, Midland, MI, USA) with a mixing ratio of 10 weight parts of the base to 1 weight part of the curing agent was used to manufacture the molds (Figure 1c). The prepolymer mixture was degassed under reduced pressure for 5 min at 2000 pm in a SpeedMixer (DAC600.2 VAC-P, Hauschild Engineering, Hamm, Germany), poured onto the master structures and subsequently cured at 75 °C for at least 3 h. After demolding, PDMS molds were used to replicate the final structures made from poly(ethyleneglycol) dimethacrylate (PEGdma600; Polysciences, Warrington, PA, USA) with an average molecular weight of 600 g mol^{-1}. 0.5 wt% 2-hydroxy-2-methylpropiophenone (Sigma-Aldrich, St. Louis, MO, USA) was mixed to the oligomer solution as a photoinitiator. A drop of the PEGdma600 oligomer solution was applied to the PDMS mold and covered with a glass slide, flushed with nitrogen for about 20 min, and then crosslinked for 300 s by UV exposure (365 nm, Omnicure S1500, Excelitas Technologies, Waltham, MA, USA).

To ensure adhesion of the PEGdma600 microstructures to the glass substrates, (3-methacryloxypropyl) trichlorosilane (AB109004, ABCR, Karlsruhe, Germany) was immobilized to the surface prior to replication. The glass substrates were rinsed in isopropanol and subsequently activated by oxygen plasma for 3 min (PICO plasma system, Diener electronic, Ebhausen, Germany). The substrates were placed together with 50 µL of silane in a vacuum chamber for about 60 min at a reduced pressure of about 50 mbar. The treated glass slides were stored in darkness and were used within two weeks.

Adhesion Measurements: Single microstructures were adhesion-tested in ambient conditions (room temperature and 55–60% relative humidity) using a Hysitron triboindenter (TI 950, Minneapolis, MN, USA). The system consisted of a force/displacement-controlled transducer coupled with an optical camera. This allowed for accurate positioning of the sample and recording of force–displacement data. All measurements were carried out with a flat diamond punch (Synton-MDP, Nidau, Switzerland) with a diameter of 50 µm. Each measurement was performed as follows. Flat punch and microstructure were brought into contact and, after a stabilization period of 45 s, the microstructure was compressed. The force was recorded while the punch was attached to the microstructure with a velocity of 240 nm s^{-1} until a preset compression depth was reached. Then, the position was held for 1 s, and the punch was pulled with the same velocity of 240 nm s^{-1} until it detached from the microstructure (Figure 2a). The maximum force necessary for detachment is the pull-off force, F_p. The pull-off stress, σ_p, was calculated by dividing the pull-off force by the apparent contact area of the structures obtained from scanning electron microscope (SEM) characterization. To evaluate pull-off stresses after comparable compressive loading, the indentation depth for each structure was chosen to correspond to the theoretical depth of the cavity as defined by the CAD model. The real depth, however, was slightly smaller due to proximity effects in the two-photon process that led to rounded corners (Figure 1b). For the structures with 180° opening angle, the pull-off force did not vary much with indentation depth (Figure S1, Supporting Information) which was thus chosen to yield similar preload stress compared to the 120° funnel structures. For in situ observation, selected experiments were performed inside a DualBeam SEM and FIB (Versa 3D DualBeam, FEI, Hillsboro, Oregon, US) equipped with a picoindenter (PI-87, Hysitron, Minneapolis, MN, USA). These tests were performed under reduced air pressure of $\approx 1.5 \times 10^{-3}$ Pa.

SEM Imaging: SEM images were taken using the SEM capabilities of the DualBeam. All samples were coated with ≈3 nm gold layer to eliminate surface charging effects. Focused ion beam cross-sections were prepared using the focused gallium ion beam at an accelerating voltage of 30 kV and a current of 3 nA. To protect the microstructures from undesired FIB damage, an ≈2 µm platinum protective stripe was first deposited on top of each microstructure. This was done using the ion beam induced deposition technique inside the DualBeam at 30 kV and 300 pA.

Numerical Simulations: Finite element simulations were performed using axisymmetric models (Comsol 5.1, COMSOL Inc., Burlington, MA, USA). The geometric parameters of the three selected models in the study were based on real dimensions obtained from the FIB cross-sections and digitally rebuilt with Solid Works 2013 (Dassault Systèmes, Vélizy-Villacoublay, France). For the simulations of the attachment, an elastic half-space (substrate) with a Poisson's ratio of 0.33 was compressed along a frictionless contact against the microstructures, which were assigned a Poisson's ratio of 0.44 and an elastic modulus of 175 MPa. The ratio of the elastic moduli between the substrate and the microstructure was 120. The microstructures were assigned hyperelastic properties based on neo-Hookean equations. For the mesh generation of the microstructures and the substrate, triangular and square elements were used, respectively. The contact was formulated as a Lagrangian contact and the substrate was defined as the receiving part of contact. The stresses within the structures as well as the stresses induced in the substrate were extracted from simulations and qualitatively analyzed with regard to the deformation behavior of the microstructures and the evolution of stress distributions along the microstructure–substrate interface.

Supporting Information

Supporting Information is available from the Wiley Online Library or from the author.

Acknowledgements

All authors contributed with conception and experimental design. K.G., O.T.A., and S.C.L.F. performed the experiments and carried out analysis of data. M.M.B. carried out the simulations and M.B. and S.F. analyzed the simulations. S.C.L.F., K.G., O.T.A., M.M.B., R.H., and E.A. wrote the paper. The authors acknowledge Robert M. McMeeking (UCSB) for helpful discussions and Birgit Heiland for performing the FIB cross-sections. The research leading to these results has received funding from the European Research Council under the European Union's Seventh Framework Programme (FP/2007-2013)/ERC Advanced Grant Agreement no. 340929.

Conflict of Interest

The authors declare no conflict of interest.

Keywords

adhesion, interfacial stress, sub-micrometer structures, two-photon lithography

Received: March 8, 2017
Revised: June 20, 2017
Published online: August 10, 2017

[1] K. Autumn, Y. A. Liang, S. T. Hsieh, W. Zesch, W. P. Chan, T. W. Kenny, R. Fearing, R. J. Full, *Nature* **2000**, *405*, 681.
[2] E. Arzt, S. Gorb, R. Spolenak, *Proc. Natl. Acad. Sci. USA* **2003**, *100*, 10603.
[3] B. N. J. Persson, *MRS Bull.* **2007**, *32*, 486.
[4] S. N. Gorb, *Functional Surfaces in Biology*, Springer, The Netherlands, **2009**.
[5] S. Chary, J. Tamelier, K. Turner, *Smart Mater. Struct.* **2013**, *22*, 025013.
[6] D. Paretkar, M. Kamperman, A. S. Schneider, D. Martina, C. Creton, E. Arzt, *Mater. Sci. Eng., C* **2011**, *31*, 1152.
[7] A. del Campo, E. Arzt, *Macromol. Biosci.* **2007**, *7*, 118.
[8] E. W. Hawkes, D. L. Christensen, H. Jiang, M. R. Cutkosky, in *2015 IEEE Int. Conf. on Robotics and Automation*, IEEE, **2015**, pp. 2305–2312.
[9] W. G. Bae, D. Kim, M. K. Kwak, L. Ha, S. M. Kang, K. Y. Suh, *Adv. Healthcare Mater.* **2013**, *2*, 109.
[10] Y. Mengüç, M. Sitti, in *Polymer Adhesion, Friction, and Lubrication*, (Ed.: H. Zeng), John Wiley & Sons, Inc., Hoboken, USA **2013**, chapter 9, pp. 351–389.
[11] V. Barreau, R. Hensel, N. K. Guimard, A. Ghatak, R. M. McMeeking, E. Arzt, *Adv. Funct. Mater.* **2016**, *26*, 4687.
[12] S. C. L. Fischer, O. Levy, E. Kroner, R. Hensel, J. M. Karp, E. Arzt, *J. Mech. Behav. Biomed. Mater.* **2016**, *61*, 87.
[13] A. del Campo, E. Arzt, *Generating Micro- and Nanopatterns on Polymeric Materials*, Wiley-VCH, Germany, **2011**.
[14] R. Hensel, R. Helbig, S. Aland, A. Voigt, C. Neinhuis, C. Werner, *NPG Asia Mater.* **2013**, *5*, e37.

[15] R. Hensel, A. Finn, R. Helbig, H. G. Braun, C. Neinhuis, W. J. Fischer, C. Werner, *Adv. Mater.* **2014**, *26*, 2029.
[16] R. Hensel, C. Neinhuis, C. Werner, *Chem. Soc. Rev.* **2016**, *45*, 323.
[17] L. Heepe, S. N. Gorb, *Annu. Rev. Mater. Res.* **2014**, *44*, 173.
[18] M. Kamperman, E. Kroner, A. del Campo, R. M. McMeeking, E. Arzt, *Adv. Eng. Mater.* **2010**, *12*, 335.
[19] G. Huber, H. Mantz, R. Spolenak, K. Mecke, K. Jacobs, S. N. Gorb, E. Arzt, *Proc. Natl. Acad. Sci. USA* **2005**, *102*, 16293.
[20] J. Israelachvili, *Intermolecular and Surface Forces*, 3rd ed., Elsevier, **2010**.
[21] V. Popov, *Kontaktmechanik Und Reibung: Ein Lehr- und Anwendungsbuch von der Nanotribologie bis zur numerischen Simulation*, Springer-Verlag, Germany, **2009**.
[22] C. Greiner, A. del Campo, E. Arzt, *Langmuir* **2007**, *23*, 3495.
[23] E. Kroner, D. R. Paretkar, R. M. McMeeking, E. Arzt, *J. Adhes.* **2011**, *87*, 447.
[24] L. F. Boesel, C. Greiner, E. Arzt, A. del Campo, *Adv. Mater.* **2010**, *22*, 2125.
[25] B. Aksak, M. P. Murphy, M. Sitti, *Langmuir* **2007**, *23*, 3322.
[26] M. Bacca, J. A. Booth, K. L. Turner, R. M. McMeeking, *J. Mech. Phys. Solids* **2016**, *96*, 428.
[27] S. N. Khaderi, N. a. Fleck, E. Arzt, R. M. McMeeking, *J. Mech. Phys. Solids* **2015**, *75*, 159.
[28] R. M. McMeeking, E. Arzt, A. G. Evans, *J. Adhes.* **2008**, *84*, 675.
[29] A. V. Spuskanyuk, R. M. McMeeking, V. S. Deshpande, E. Arzt, *Acta Biomater.* **2008**, *4*, 1669.
[30] H. Gao, H. Yao, *Proc. Natl. Acad. Sci. USA* **2004**, *101*, 7851.
[31] G. Carbone, E. Pierro, *Small* **2012**, *8*, 1449.
[32] L. Heepe, A. E. Kovalev, A. E. Filippov, S. N. Gorb, *Phys. Rev. Lett.* **2013**, *111*, 104301.
[33] R. G. G. Balijepalli, M. R. R. Begley, N. A. A. Fleck, R. M. M. McMeeking, E. Arzt, *Int. J. Solids Struct.* **2016**, *85*, 160.
[34] B. Aksak, K. Sahin, M. Sitti, *Beilstein J. Nanotechnol.* **2014**, *5*, 630.
[35] L. Heepe, A. E. Kovalev, M. Varenberg, J. Tuma, S. N. Gorb, *Theor. Appl. Mech. Lett.* **2012**, *2*, 014008.
[36] E. Kroner, E. Arzt, *Int. J. Adhes. Adhes.* **2012**, *36*, 32.
[37] C. Greiner, R. Spolenak, E. Arzt, *Acta Biomater.* **2009**, *5*, 597.
[38] R. Spolenak, S. Gorb, H. Gao, E. Arzt, *Proc. R. Soc. London, Ser. A* **2005**, *461*, 305.
[39] A. del Campo, C. Greiner, E. Arzt, *Langmuir* **2007**, *23*, 10235.
[40] M. K. Kwak, H. E. Jeong, W. G. Bae, H. S. Jung, K. Y. Suh, *Small* **2011**, *7*, 2296.
[41] M. Varenberg, N. M. Pugno, S. N. Gorb, *Soft Matter* **2010**, *6*, 3269.
[42] S. Kim, M. Sitti, *Appl. Phys. Lett.* **2006**, *89*, 261911.
[43] H. E. Jeong, J. K. Lee, M. K. Kwak, S. H. Moon, K. Y. Suh, *Appl. Phys. Lett.* **2010**, *96*, 043704.
[44] H. E. Jeong, J.-K. Lee, H. N. Kim, S. H. Moon, K. Y. Suh, *Proc. Natl. Acad. Sci. USA* **2009**, *106*, 5639.
[45] R. G. Balijepalli, S. C. L. Fischer, R. Hensel, R. M. McMeeking, E. Arzt, *J. Mech. Phys. Solids* **2017**, *99*, 357.
[46] S. C. L. Fischer, E. Arzt, R. Hensel, *ACS Appl. Mater. Interfaces* **2017**, *9*, 1036.
[47] S. Cheng, M. O. Robbins, *Phys. Rev. E: Stat., Nonlinear, Soft Matter Phys.* **2014**, *89*, 062402.
[48] H. Yi, I. Hwang, J. H. Lee, D. Lee, H. Lim, D. Tahk, M. Sung, W.-G. Bae, S.-J. Choi, M. K. Kwak, H. E. Jeong, *ACS Appl. Mater. Interfaces* **2014**, *6*, 14590.
[49] D. Sameoto, B. Ferguson, *J. Adhes. Sci. Technol.* **2014**, *28*, 337.
[50] D. Labonte, W. Federle, *Philos. Trans. R. Soc., B* **2015**, *370*, 20140027.
[51] K. Autumn, A. Dittmore, D. Santos, M. Spenko, M. Cutkosky, *J. Exp. Biol.* **2006**, *209*, 3569.
[52] H. Zeng, N. Pesika, Y. Tian, B. Zhao, Y. Chen, M. Tirrell, K. L. Turner, J. N. Israelachvili, *Langmuir* **2009**, *25*, 7486.
[53] R. M. McMeeking, L. Ma, E. Arzt, *Adv. Eng. Mater.* **2010**, *12*, 389.